European Cells and Materials Vol. 36 2018 (pages 69-80) DOI: 10.22203/eCM.v036a06 ISSN 1473-2262

OSTEOGENIC EXTRACELLULAR MATRIX SHEET FOR BONE TISSUE REGENERATION

T. Onishi[1,*], T. Shimizu[2], M. Akahane[3], S. Omokawa[4], A. Okuda[5], T. Kira[2], Y. Inagaki[6] and Y. Tanaka[2]

[1] Department of Orthopaedic Surgery, Higashiosaka City Medical Centre, Higashiosaka, Japan
[2] Department of Orthopaedic Surgery, Nara Medical University, Kashihara, Japan
[3] Department of Public Health, Health Management and Policy, Nara Medical University, Faculty of Medicine, Kashihara, Japan
[4] Department of Hand Surgery, Nara Medical University, Kashihara, Japan
[5] Department of Emergency, Nara Medical University, Kashihara, Japan
[6] Department of Artificial Joint and Regenerative Medicine, Nara Medical University, Kashihara, Japan

Abstract

The application of extracellular matrix (ECM) sheets without a scaffold is not extensively reported in bone regenerative medicine. The aim of the present study was to demonstrate that an osteogenic ECM sheet (OECMS) can retain ECM integrity and growth factors to enhance bone formation in a rat non-union model. The OECMS was produced from osteogenic cell sheets (OCS). Collagen and growth factor [bone morphogenetic protein 2 (BMP-2), vascular endothelial growth factors (VFGFs), basic fibroblast growth factor (bFGF) and transforming growth factor β1 (TGF-β1)] concentrations in the OECMS were quantified by enzyme-linked immunosorbent assay (ELISA). Next, hydroxyapatite (HA) constructs combined with OECMSs were implanted subcutaneously into the rats' backs to evaluate their osteoinductive capacity by histological evaluation. In addition, OECMSs were implanted in a rat femoral non-union model. 18 male Fischer 344 inbred rats were divided into OECMS and control groups. Fracture healing was evaluated by radiological and histological analyses at 2, 5 and 8 weeks and biological analysis at 8 weeks. Collagen I and growth factors were retained in the OECMSs. Osteoid formation was identified in the HA combined with OECMS at 4 weeks. Enhanced bone regeneration at the non-union of the OECMS group was confirmed at 5 and 8 weeks. Biomechanical testing revealed a significantly higher maximum bending load in the OECMS group as compared to the control group at 8 weeks. The results demonstrated that the OECMS retained BMP-2 and TGF-β1 and high osteoinductive and osteoconductive capacity. As such, the OECMS represents a potential new scaffold-free material for bone tissue engineering.

Keywords: Extracellular matrix, cell sheet, osteoinductive capacity, osteoconductive capacity, bone regeneration, non-union model.

***Address for correspondence**: Takamasa Shimizu, M.D., Department of Orthopaedic Surgery, Nara Medical University, 840 Shijo-cho, Kashihara, Nara, 634-8522, Japan.
Email: tk-shimi@naramed-u.ac.jp

Introduction

Bone regeneration requires a sequence of biological events such as cellular recruitment, proliferation and differentiation. At the molecular level, several mediators and cellular elements facilitate the initiation and evolution of the bone regeneration process, with the interactions among osteoprogenitor cells, growth factors and the extracellular matrix (ECM) playing an important role in creating the foundation for successful bone healing (Schindeler *et al.*, 2008). Various types of biomaterials are currently used for bone regeneration, with optimal bone regeneration requiring both an osteoconductive matrix, as well as osteoinductive factors and osteogenic cells (Giannoudis *et al.*, 2007). Therefore, the combination of osteoinductive growth factors and/or stem/progenitor cells with osteoconductive biomaterials is a promising approach to promote bone regeneration.

Although stem/progenitor cells are effective in enhancing bone regeneration, their clinical application is limited by the negative effects of aging on the number, replication and osteogenesis of stem/progenitor cells (Sun *et al.*, 2011). Growth factors also have the capacity to promote bone regeneration, with several products containing recombinant growth factors being used in orthopaedic applications, such as for spinal fusions, non-unions and oral surgery (Axelrad *et al.*, 2009; Even *et al.*, 2012). However, growth factors are not widely used in practice due to issues of safety and costs. Therefore, there is a need for the development of delivery systems that can provide a safe and cost-effective way to deliver a high dose of growth factors locally. The application of cell-derived ECM in tissue engineering has gained increasing interest in this matter.

The ECM is rich in collagen and proteoglycans and provides a natural scaffold for all cellular events and interactions involved in bone regeneration (Komatsu *et al.*, 2010; Zhang *et al.*, 2016), as well as being a repository for a variety of different growth factors (Dischер *et al.*, 2009; Macri *et al.*, 2007; Schultz *et al.*, 2009). Several studies show that composite 3D hybrid scaffolds, composed of various types of inorganic materials [collagen/hydroxyapatite (Col/HA), poly(lactic-co-glycolic acid)/poly(lactic acid) (PLGA/PLA) and Ti fibre], in combination with cell-derived ECM promote osteogenesis and bone healing (Antebi *et al.*, 2015; Kim *et al.*, 2015; Pham *et al.*, 2008). Some groups have attempted to develop cellular sheets made of autologous ECM and living cells without an artificial scaffold to overcome the complications of cell-derived ECM hybrid artificial scaffolds, including the production of harmful degradation products, asynchronous scaffold absorption and bone regeneration (Kittaka *et al.*, 2015; Lau *et al.*, 2012).

An osteogenic cell sheet (OCS), fabricated from bone marrow stromal cells (BMSCs), contains enriched osteoblasts, ECM and growth factors, including bone morphogenetic protein 2 (BMP-2) and vascular endothelial growth factor (VFGF) (Shimizu *et al.*, 2015). These OCSs can form bone tissue without a scaffold (Nakamura *et al.*, 2010), as well as enhancing bone regeneration in a critical fracture-healing model (Shimizu *et al.*, 2015). However, the application of ECM sheets without an artificial scaffold is reported in a few cases, particularly in the field of bone tissue engineering (Kittaka *et al.*, 2015; Lau *et al.*, 2012). ECM sheets without artificial scaffold and cell seeding have the potential to enhance the bone healing response (Zhang *et al.*, 2016) and, as such, are important to study as they could provide a novel biomaterial for bone tissue engineering. Therefore, the aim of the current study was to evaluate experimentally the osteogenic capacity of osteogenic ECM sheets (OECMSs) and to determine if they retain their ECM and growth factor integrity after implantation for enhanced bone regeneration.

Materials and Methods

Study design

OECMSs were produced *in vitro* from OCSs using a process involving cooling in liquid nitrogen. Next, OECMSs were implanted together with the HA constructs subcutaneously into the recipient rats' backs to assess their osteoinductive capacity, by biochemical and histological assessment, 4 weeks after implantation. In a second *in vivo* study, two OECMSs were implanted in a rat model of femoral non-union. 18 male Fischer 344 inbred rats were divided into two groups, OECMS and control ($n = 9$ each). Fracture healing was evaluated by radiological and histological analysis at 2, 5 and 8 weeks ($n = 1$ in each group). Biological analysis was also performed at 8 weeks ($n = 6$ in each group). The research protocol was approved by the Institutional Animal Care and Use Committee of Nara Medical University, Japan following appropriate guidelines (Nr. 11199).

In vitro study

Preparation of the OECMS

BMSCs were prepared as previously described (Akahane *et al.*, 2008; Akahane *et al.*, 2010; Nakamura *et al.*, 2010). The standard culture medium consisted of minimal essential medium (Nacalai Tesque Inc., Kyoto, Japan) containing 15 % foetal bovine serum (172012; Sigma-Aldrich) and antibiotics (100 U/mL penicillin and 100 mg/mL streptomycin, Nacalai Tesque Inc.). Then, BMSCs were transferred into two T-75 flasks (Falcon) containing 15 mL of standard culture medium. After reaching confluence, cultured cells were detached from the culture substratum using trypsin/ethylenediamine tetra-acetic acid (EDTA) (Nacalai Tesque Inc.). They were seeded at a cell density of 1×10^4 cells/cm^2 in a 10 cm dish (100 mm × 20 mm; Falcon) and cultured in a standard medium with 10 nM dexamethasone (Dex, Sigma-Aldrich) and 0.28 mM of ascorbic acid phosphate (Wako Pure Chemical Industries, Ltd., Osaka, Japan).

Fabrication and cell viability in the OECMS

After 14 d, the ECMs were lifted as an OCS, using a cell scraper. The OCS was soaked for 1 min in liquid nitrogen (− 196 °C) using forceps, thawed in 37 °C phosphate-buffered saline (PBS) and rinsed with PBS until the OCS regained its original shape. After two repetitions of this cycle, the OCS was used for implantation as OECMS.

To investigate the viability of the OECMS, a method based on tetrazolium reductase activity (Cell Counting Kit-8®; WST-8, Dojindo, Kumamoto, Japan) was employed (Kito *et al.*, 2005). Briefly, OCSs cultured in 6-, 12-, 24- and 48-well plates (BD Falcon; $n = 6$ per plate) were used to generate the standards. The differently sized OCSs were harvested with a scraper and incubated for 24 h at 37 °C in a 95 % humidified atmosphere with 5 % CO_2. Then, the samples were placed in WST-8 solution (100 µL in

1 mL of culture medium) in culture wells. After 3 h of incubation, the solution obtained from each culture well was analysed by spectrophotometry (450 nm). Based on the standardisation, a linear relationship was obtained between the average optical density and the seeded cell number per volume of culture medium (cell/mL) (correlation $R^2 = 0.975$). Using this standard, the cell viability of the OECMS was analysed.

Collagen immunocytochemical staining

Histological and cytological immunostainings were performed as previously described (Okuda *et al.*, 2017). In brief, cultured cells, plated on poly-D-lysine-coated coverslips, were fixed with 4 % paraformaldehyde in 0.1 M phosphate buffer (pH 7.4) for 10 min. After permeabilisation with 0.3 % Triton X-100 in PBS (PBST), cells were blocked with 5 % normal horse serum in PBST and incubated with rabbit anti-collagen I (1 : 200; Abcam). Cells were further incubated with species-specific secondary antibodies conjugated with CF-555 (1 : 1000; BiotiumaaA, Hayward, CA, USA). All immunocytochemical images were captured using a FluoView 1000 confocal microscope (Olympus) with a 512 × 512 pixels array.

Collagen and growth factors quantification

Cell lysates were prepared using a mammalian protein extraction reagent (m-PeR; Pierce, Rockford, IL, USA) containing a protease inhibitor cocktail (1 mm sodium orthovanadate and 25 mm sodium fluoride). The protein concentration was measured twice using a BCA Protein Assay Kit (Pierce), with bovine serum albumin as the standard. Cell lysate samples, containing 10 μg of protein, were separated by sodium dodecyl sulphate (SDS)-polyacrylamide gel electrophoresis and transferred to a polyvinylidene difluoride membrane (Invitrogen). The concentration of collagen I and growth factors, including BMP-2, vascular endothelial growth factor A (VEGF-A), basic fibroblast growth factor (bFGF) and transforming growth factor β1 (TGF-β1), was quantified in the samples using the ELISA method. Aliquots of the samples ($n = 6$ for each protein) were analysed using Quantikine ELISA kits to determine the specific concentration of collagen I (Mouse Pro-Collagen I alpha 1 ELISA Kit, ab210579, Abcam), BMP-2 (Rat BMP-2 Quantikine ELISA Kit, DBP200, R&D Systems Inc.), VEGF-A (Rat VEGF Quantikine ELISA Kit, RRV00, R&D Systems Inc.), bFGF (Rat bFGF Quantikine ELISA Kit, MFB00, R&D Systems Inc.) and TGF-β1 (Rat TGF-β1 Quantikine ELISA Kit, MB100B, R&D Systems Inc.).

In vivo study

Implantation of hydroxyapatite (HA) ceramics combined with OECMS

Porous HA ceramics (50 % average void volume, 5 mm diameter, 2 mm thickness; Cellyard HA scaffold, Pentax Co, Tokyo, Japan) were used for implantation. Both solid and porous components of the scaffold microstructure were interconnected. HA ceramics combined with or without the OECMS were implanted in the recipient rats' backs. Each group included 6 constructs to assess the osteogenic potential of the OECMS ($n = 6$ HA disks per rat).

Biochemical analysis of the HA constructs

Total RNA was extracted from harvested specimens (HA ceramics without sheet: control group; HA ceramics with OECMS: OECMS group) at 4 weeks after implantation using ISOGEN (Nippon Gene, Tokyo, Japan) and reverse-transcribed into complementary DNA. Real-time quantitative polymerase chain reaction (TaqMan; Life Technologies) was conducted to measure mRNA expression levels of alkaline phosphatase (Rn00564931m1) and osteocalcin (Rn01455285g1) using primers and specific fluorogenic probes ($n = 6$ for each group at 4 weeks after implantation). Thermal cycling conditions were as follows: 20 s at 95 °C for activation (TaqMan Fast Universal PCR Master Mix, Thermo Fisher Scientific), 40 cycles of 1 s at 95 °C for denaturation and 20 s at 60 °C for annealing and extension. Target mRNA levels were compared after correcting to the glyceraldehyde-3-phosphate dehydrogenase (*GAPDH*) (Rn99999916s1) mRNA levels as an internal standard, which was used to adjust the differences in the efficiency of reverse transcription among samples.

Histological analysis of the HA constructs

One HA construct in each group was harvested for histological evaluation at 2 and 4 weeks after implantation. The samples were fixed for 4 d in 10 % normal buffered formaldehyde, decalcified in EDTA, dehydrated with ethanol and embedded in a methyl methacrylate (MMA) resin. 4 μm-thick cross-sections were obtained using a wet slicing method performed with an automatic rotary microtome (RM2255, Leica Microsystems). The sections were deresined with xylene and stained with a Villanueva-Goldner stain for histological observation [$n = 1$ for each time point (2 and 4 weeks) in each group].

Implantation of the OECMS in a non-union rat femur model

A rat non-union model was created by modifying the method described by Kokubu *et al.* (2003). 12-week-old male Fischer 344 inbred rats (approximately 280 g) were anesthetised with 2 % isoflurane. A 30 mm-long lateral incision was made on the hind limb and a fracture was created by transverse osteotomy with an oscillating mini saw. The periosteum was cauterised circumferentially with a 2 mm margin on each side of the fracture. The femur was fixed intradmedullary with a K-wire (1.25 mm in diameter), according to the method described by Kokubu *et al.* (2003) (Fig. 1**a**). Then, 18 rats were divided into two groups: untreated and OECMS group. In the OECMS group, two OECMSs were implanted at the fracture site of the femur

(Fig. 1**b**). Unprotected weight bearing was allowed immediately after the operation. Postoperative pain was managed through subcutaneous administration of buprenorphine hydrochloride. Postoperative antibiotics were prophylactically administered by intramuscular injection of penicillin. Radiological, histological and biomechanical analyses were performed.

Radiological analysis of rat femora

Radiographs of the rats in the two groups were taken 2, 5 and 8 weeks after surgery. Under anaesthesia, animals were placed in a prone position with both limbs fully abducted and externally rotated. Radiographic fracture unions were evaluated at 2, 5 and 8 weeks and the union rates were tabulated. Fracture union was determined by the presence of bridging callus on two cortices [$n = 1$ for each time point (2, 5 and 8 weeks) in each group].

Histological analyses of rat femora

One rat in each group was utilised for histological evaluation at 2, 5 and 8 weeks after surgery. The harvested femurs were fixed for 4 d in 10 % normal buffered formaldehyde, decalcified in EDTA, dehydrated with ethanol and embedded in MMA resin. 4 μm-thick cross-sections were obtained using a wet slicing method with a fully automatic rotary microtome [Micro cutting machine (BS-300CL), micro grinding machine (MG-400CS); EXAKT; Oklahoma City, OK, USA]. The sections were deresined with xylene and stained with a Villanueva-Goldner stain for histological observation [$n = 1$ for each time point (2, 5 and 8 weeks) in each group].

Biomechanical analysis of rat femora

6 rat femora in each group were harvested 8 weeks after surgery. The femora were subjected to standardised three-point bending tests, performed using a universal testing machine (TRI/3D-BON-RATOC System Engineering Co., Ltd., Tokyo, Japan). The cross-head speed was 10 mm/min, with the maximum bending load-to-rupture determined as the ultimate load. The ultimate stress (N), extrinsic stiffness (N/mm) and failure energy (N × mm) were interpreted and calculated from the load deflection curve ($n = 6$ for each group at 8 weeks).

Statistical analysis

All values are expressed as mean ± standard deviation. The Mann-Whitney U-test was used for comparisons between two experimental groups. Data analysis was conducted using the Statistical Package for Social Science (SPSS) software package (version 17.0; SPSS Inc., Chicago, IL, USA). A probability value of $p < 0.05$ was considered statistically significant.

Results

***In vitro* study**

Cell viability in the OECMS group

Cell viability in the OECMS group (0.2 %) was significantly decreased as compared to the OCS group (mean absorbance: OCS, 2.0 ± 0.2; OECMS, 0.0055 ± 0.0036; $p < 0.001$).

Collagen I immunocytochemical staining and quantification of OCS and OECMS

The immunocytochemical staining for collagen I showed that the collagen component was preserved in both OCS and OECMS. The fibrous sheet structure of the OECMS was not broken into small fragments after the freeze-thaw procedure in liquid nitrogen (Fig. 2**a**). Collagen I was retained in the OECMS group, with the mean concentration being not significantly different between the two groups (OCS, 959.9 ± 69.7 ng/mL; OECMS, 889.3 ± 62.0 ng/mL; $p = 0.12$; Fig. 2**b**).

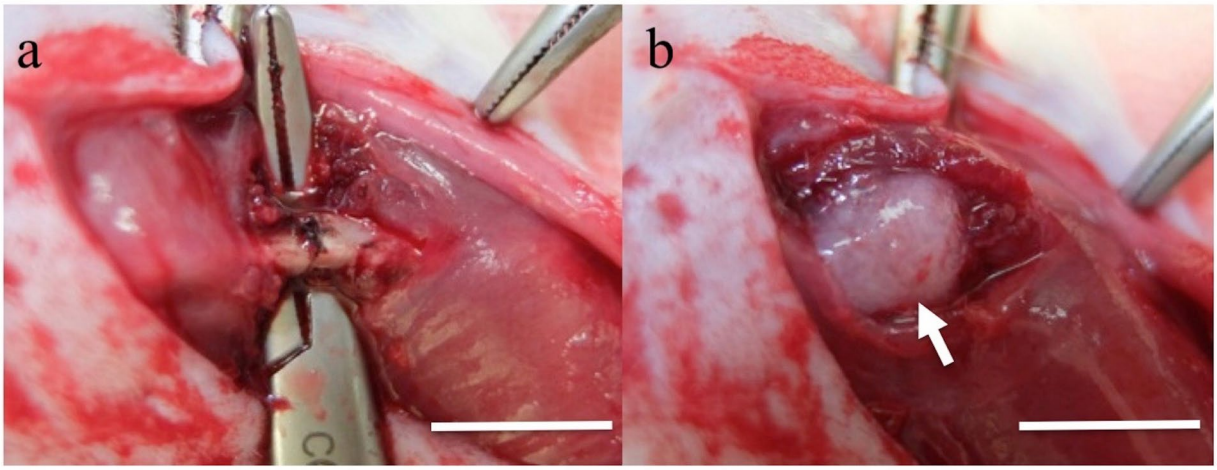

Fig. 1. Implantation of osteogenic extracellular matrix sheet in a rat model of fracture non-union of the femur. (**a**) The periosteum was cauterised circumferentially with a 2 mm margin on each side of the fracture site. (**b**) Implantation of osteogenic extracellular matrix sheet (white arrow) at the fracture site of the rat femur. Scale bar = 5 mm.

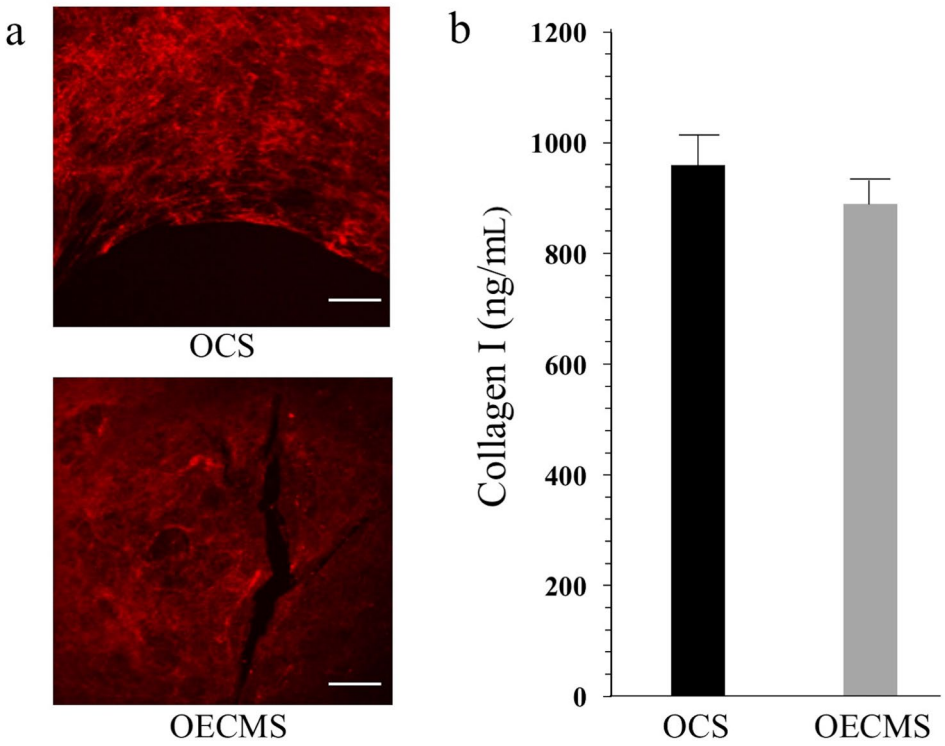

Fig. 2. Collagen I immunocytochemical staining and quantification of OCS and OECMS. (**a**) Characterisation of collagen I before and after freeze-thaw cycling in liquid nitrogen using immunocytochemical staining. Collagen I was observed in both OCS and OECMS. The fibrous structure of the OECMS was not broken to small fragments after freeze-thaw cycling. Scale bar = 100 μm. (**b**) Collagen I quantification showing preservation of collagen content after the freeze-thaw procedure ($n = 6$).

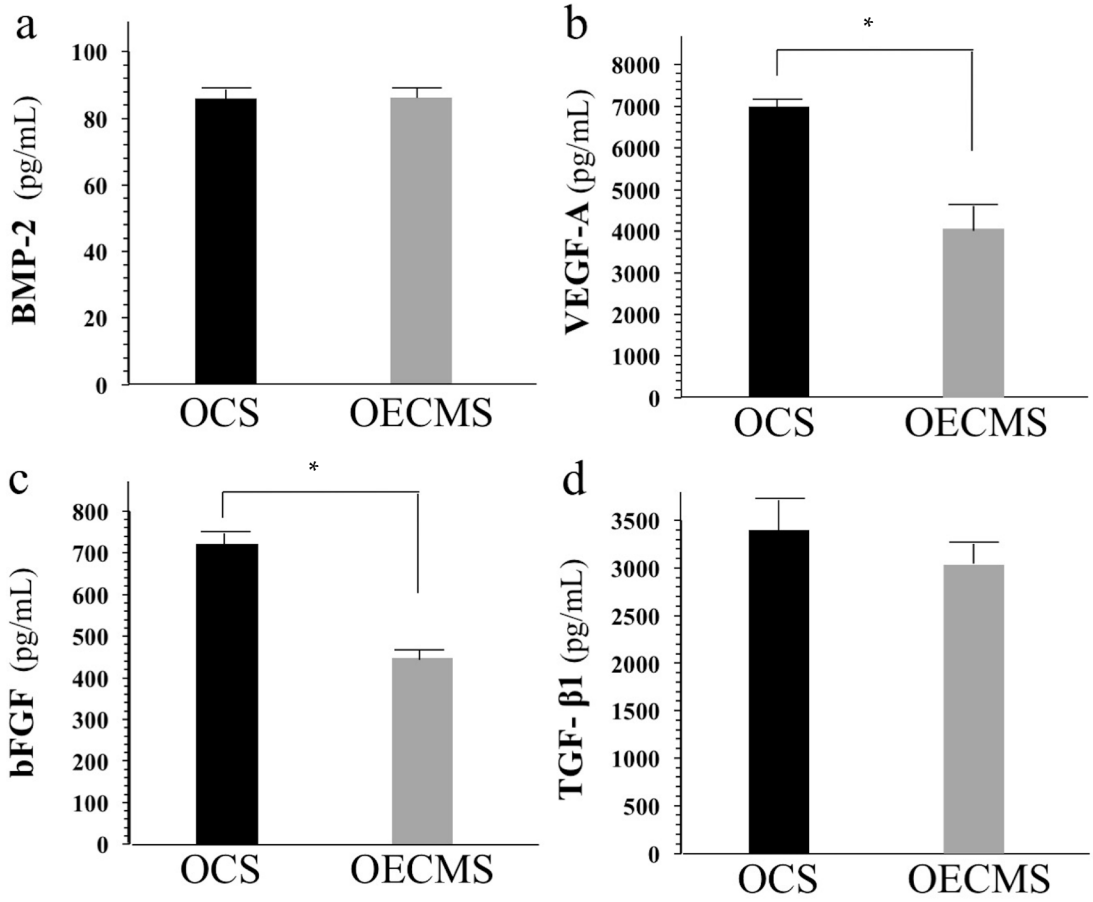

Fig. 3. Quantified content of growth factors, including BMP-2, VEGF-A, bFGF and TGF-β1. Growth factors were preserved after freeze-thaw cycling in liquid nitrogen (* $p < 0.05$, $n = 6$).

Growth factors quantification of OCS and OECMS

Growth factor content was retained in the OCS and OECMS groups (BMP-2: OCS, 86.1 ± 3.6 pg/mL; OECMS, 86.3 ± 2.0 pg/mL. VFGF-A: OCS, 6944.3 ± 252.2 pg/mL; OECMS, 4055.9 ± 362.9 pg/mL. bFGF: OCS, 720.4 ± 67.4 pg/mL; OECMS, 448.4 ± 43.7 pg/mL. TGF-β1: OCS, 3400.2 ± 381.7 pg/mL; OECMS, 3037 ± 186.2 pg/mL; Fig. 3). The mean concentration of VEGF-A and bFGF were significantly decreased after the freeze-thaw procedure in liquid nitrogen.

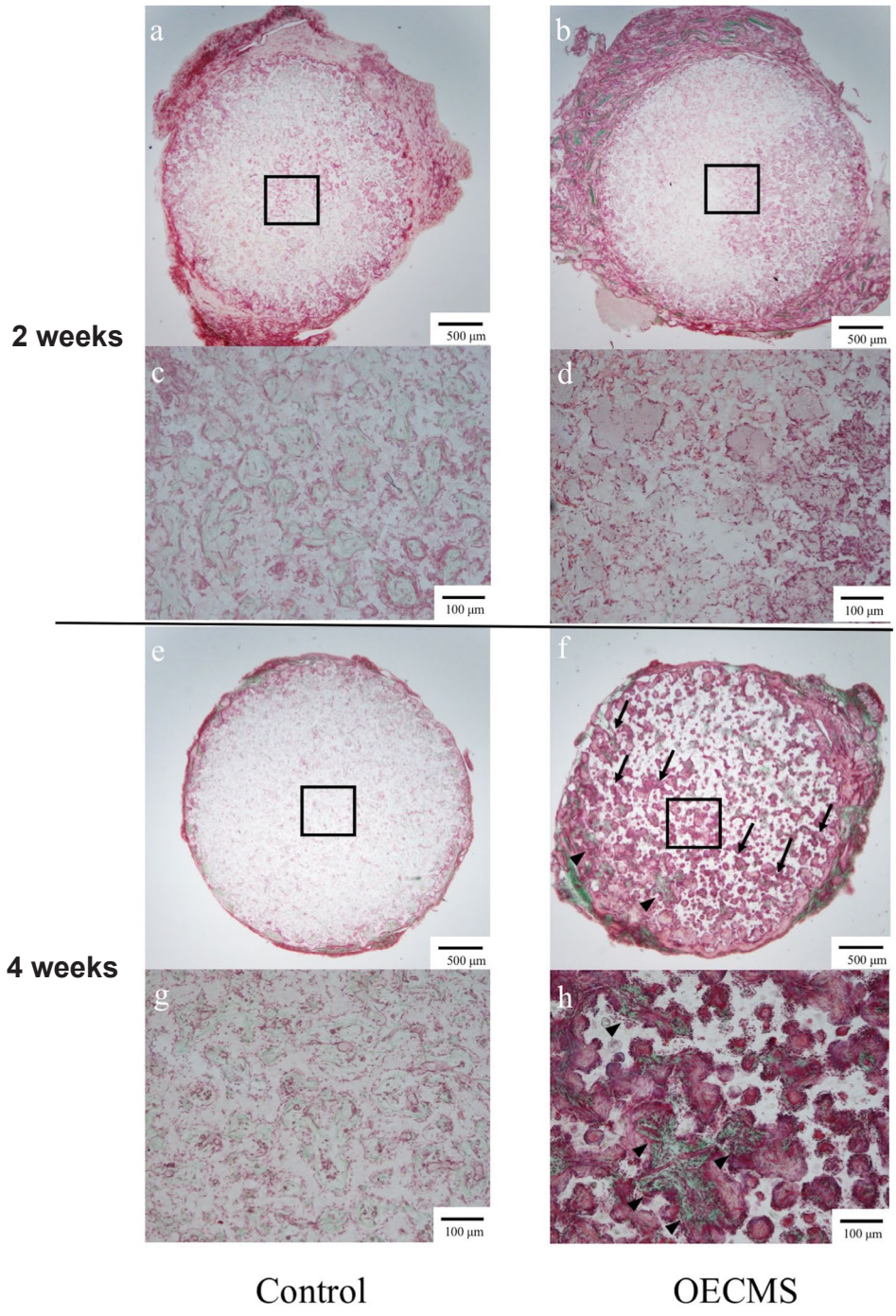

Fig. 4. Histological examination of the harvested HA constructs stained with Villanueva-Goldner staining. (**b**,**d**) 2 weeks after implantation, in the OECMS group, HA was surrounded by osteoid (red staining) and calcification (green staining), originating from the implanted OECMS; however, there was little osteoid formation and calcification inside the HA. (**c**,**d**) There was no difference in the amount of osteoid and calcification inside the HA between the control and OECMS groups. (**f**,**h**) 4 weeks after implantation, in the OECMS group, the amount of osteoid formation (red staining: black arrow) and calcification (green staining: black arrow head) inside the HA increased. (**a**,**c**,**e**,**g**) In the control groups, little osteoid formation and calcification was observed inside the HA pores both 2 and 4 weeks after implantation.

***In vivo* study**

Biochemical evaluation of the HA constructs

The mRNA expression levels in the constructs 4 weeks after implantation were assessed by real-time quantitative polymerase chain reaction. The mRNA level of osteocalcin was significantly lower in the OECMS and control groups than in the OCS group (control group: 0.0001 pg/fg *GAPDH*; OECMS group: 0.00028 pg/fg *GAPDH*). The mRNA level of alkaline phosphatase was significantly lower in the OECMS and control groups than in the OCS group (control group: 0.0015 pg/fg *GAPDH*; OECMS group: 0.00047 pg/fg *GAPDH*).

Histological examination of the HA constructs

2 weeks after implantation, in the OECMS group, the HA was surrounded by an osteoid (red staining) and calcification (green staining) originating from the implanted OECMS, but little osteoid formation and calcification was present inside the HA (Fig. 4**b**,**d**). No difference in the amount of osteoid and calcification inside the HA were observed between the control and OECMS groups (Fig. 4**c**,**d**). On the other hand, 4 weeks after implantation, the amount of osteoid formation (red staining: black arrow) and calcification (green staining: black arrow head) inside the HA increased in the OECMS group (Fig. 4**f**,**h**). In the control group, little osteoid formation and calcification was observed inside the HA pores 2 and 4 weeks after implantation (Fig. 4**a**,**c**,**e**,**g**).

Radiological findings of rat femora

Radiographs taken just after surgery showed a transverse mid-shaft femoral osteotomy in both groups (Fig. 5**a**,**d**). The OECMS group displayed abundant callus formation (black arrow) around the fracture site 5 weeks after implantation. The posterior callus bridged both ends of the fractured bone and the cortical gap on both sides of the defect site disappeared (Fig. 5**e**). This was followed by callus consolidation (black arrowhead) by week 8 (Fig. 5**f**). In comparison, the control group showed a lack of vigorous callus formation around the fracture site at 5 weeks (Fig. 5**b**). By 8 weeks, the ends of the fractured bone had become rounded and were resorbed, giving the appearance of typical established non-union (Fig. 5**c**).

Table 1 shows the numbers of radiographic fracture unions during each period. Union was achieved in almost all the rat femora (86 %) in the OECMS group at week 8 after implantation, a rate that was significantly higher than in the control group (0 %).

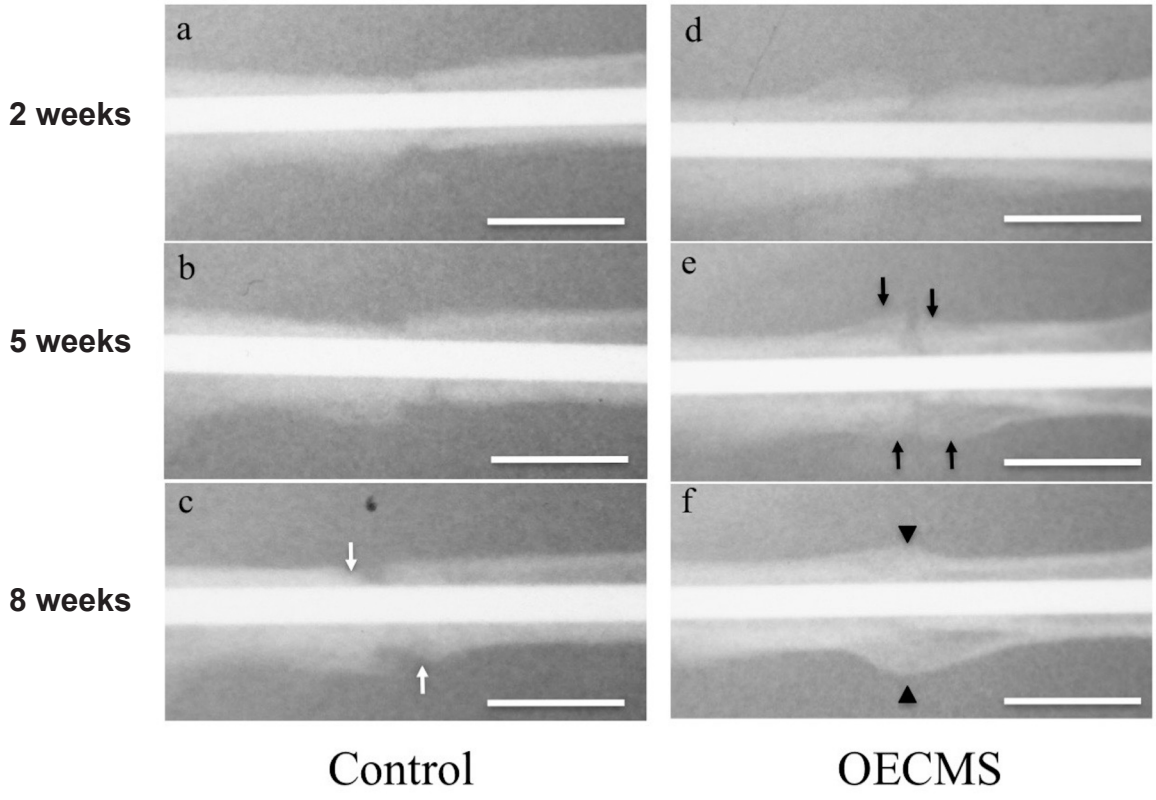

Fig. 5. Representative radiographs of fracture sites at 2, 5 and 8 weeks in OECMS and control groups. (**e**) The OECMS group displayed abundant callus formation (black arrow) around the fractures site 5 weeks after implantation. (**f**) This was later followed by callus consolidation (black arrow head) by 8 weeks. (**b**) By comparison, the control group showed a small amount of callus formation along the periosteum, away from the fracture site at 5 weeks. (**c**) By 8 weeks, the ends of the fractured bone had become rounded and were resorbed (white arrow), giving the appearance of typical established non-union. Scale bar = 5 mm.

Table 1. Radiographic fracture unions during each period. Fracture union was determined by the presence of bridging callus on two cortices. Union was achieved in almost all the rat femurs (86 %) in the OECMS group 8 weeks after implantation, a rate that was significantly higher than in the control group (0 %).

Time after surgery	Control	OECMS
2 weeks	0/9 (0 %)	0/9 (0 %)
5 weeks	0/8 (0 %)	3/8 (38 %)
8 weeks	0/7 (0 %)	6/7 (86 %)

Histological findings of rat femora

2 weeks after surgery, the OECMS group presented large soft tissue covering the fracture site and a small amount of calcification (green staining: black arrow) in the outer layer of the covering tissue (Fig. 6**b**). In contrast, the control group showed a fibrous tissue (☆) interposition between the ends of the fractured bone (Fig. 6**a**). At 5 weeks, the obvious calcification (green staining: black arrowhead) was expanded onto the periosteum in the OECMS group (Fig. 6**d**). However, the bridging calcification was not confirmed over the fracture site in the control group (Fig. 6**c**). 8 weeks after surgery, bridging callus over the fracture site was observed in the OECMS group (Fig. 6**f**). However, the control group showed fibrous granulation tissue (☆) at the fracture site, the ends of cortical bone had become rounded and there was evidence of bony resorption (Fig. 6**e**).

Biomechanical results of rat femora

The maximum bending load in the experimental femora was determined across the course of the study, as reported by Shimizu *et al.* (2010). In cases where the experimental femurs did not rupture in the three-point bending tests, the provisional maximum bending load was determined to be the load required to rupture the intact contralateral femur (deflection of 1.2 mm). The maximum bending load in the OECMS group was significantly higher than in the control group [OECMS: 45.2 ± 24 N (range: 9.52-75.0 N); control: 10.3 ± 9.6 N (range: 0.85-22.4 N); $p < 0.05$]. The stiffness in the OECMS group was higher than in the control group [OECMS: 116 ± 99 N/mm (range: 35-271 N/mm); control: 25.7 ± 21 N/mm (range: 0-55 N/mm); $p = 0.07$]. The failure energy in the OECMS group was significantly higher than in the control group [OECMS: 12.2 ± 5.3 N × mm (range: 2-18 N × mm); control: 3.1 ± 3.5 N × mm (range: 0.24-8.5 N × mm); $p < 0.05$; Fig. 7].

Discussion

The cell viability of the OECMS was 0.2 % when compared with the OCS. OECMSs were almost completely devitalised and maintained their original shape and autogenous proteins after the freeze-thaw cycling in liquid nitrogen. ECM sheets are produced by various decellularisation protocols and contain several growth factors (Farag *et al.*, 2014; Junka *et al.*, 2015; Kim *et al.*, 2012; Xing *et al.*, 2015). Xing *et al.* (2015) report that the freeze-thaw cycling procedure applied to fibroblast-cell-derived ECM sheets preserves the ECM molecules and maintains the ECM structure, as well as its mechanical strength, compared with chemical treatment using high and low concentrations of SDS. As previously reported, the freeze-thaw cycling procedure does not negatively affect the sheet shape and the amount of retained collagen I (Xing *et al.*, 2015).

A considerable number of growth factors, including BMP-2, VEGF-A, bFGF and TGF-β1, were also retained in the OECMS. Pro-angiogenic factors, including VEGFs, bFGF and BMPs, promote angiogenesis within the soft callus (Fei *et al.*, 2013; Hankenson *et al.*, 2011). Tsuchiya *et al.* (2005) report that frozen autografts treated in liquid nitrogen contain autogenous proteins, growth factors and cytokines and do not elicit an immune reaction. Takata *et al.* (2011) report the amount and activity of BMP-7 extracted from human femoral bone after treatment with hyper- and hypothermia – including the temperature groups − 196, − 73, 60, 321, 100 and 4 °C (as control) – with the maximum percentage of BMP-7 being 114 % (where the value of the control group is set at 100 %) in the − 196 °C group, as measured by ELISA assay. Xing *et al.* (2015) show that freeze-thaw treatments can preserve much more growth factors, including VEGF-A and FGF-2, than chemical treatment using high concentrations of SDS. Osteoinductive growth factors can be maintained after freeze-thaw cycling in liquid nitrogen, which has advantages in producing OECMS.

In the OECMS group, 2 weeks after implantation, the HA constructs were surrounded by osteoid and calcification originated from the implanted OECMS. However, there was little osteoid formation and calcification inside the HA, which was comparable to the control group. These results indicated that osteoid formation, deposited in previous stages of the *in vitro* culture by the BMSCs, could not progress inside the HA in the early stage after implantation. On the other hand, in the OECMS group, the amount of osteoid formation and calcification inside the HA increased 4 weeks after implantation, differently from the control group. The osteoid and calcification

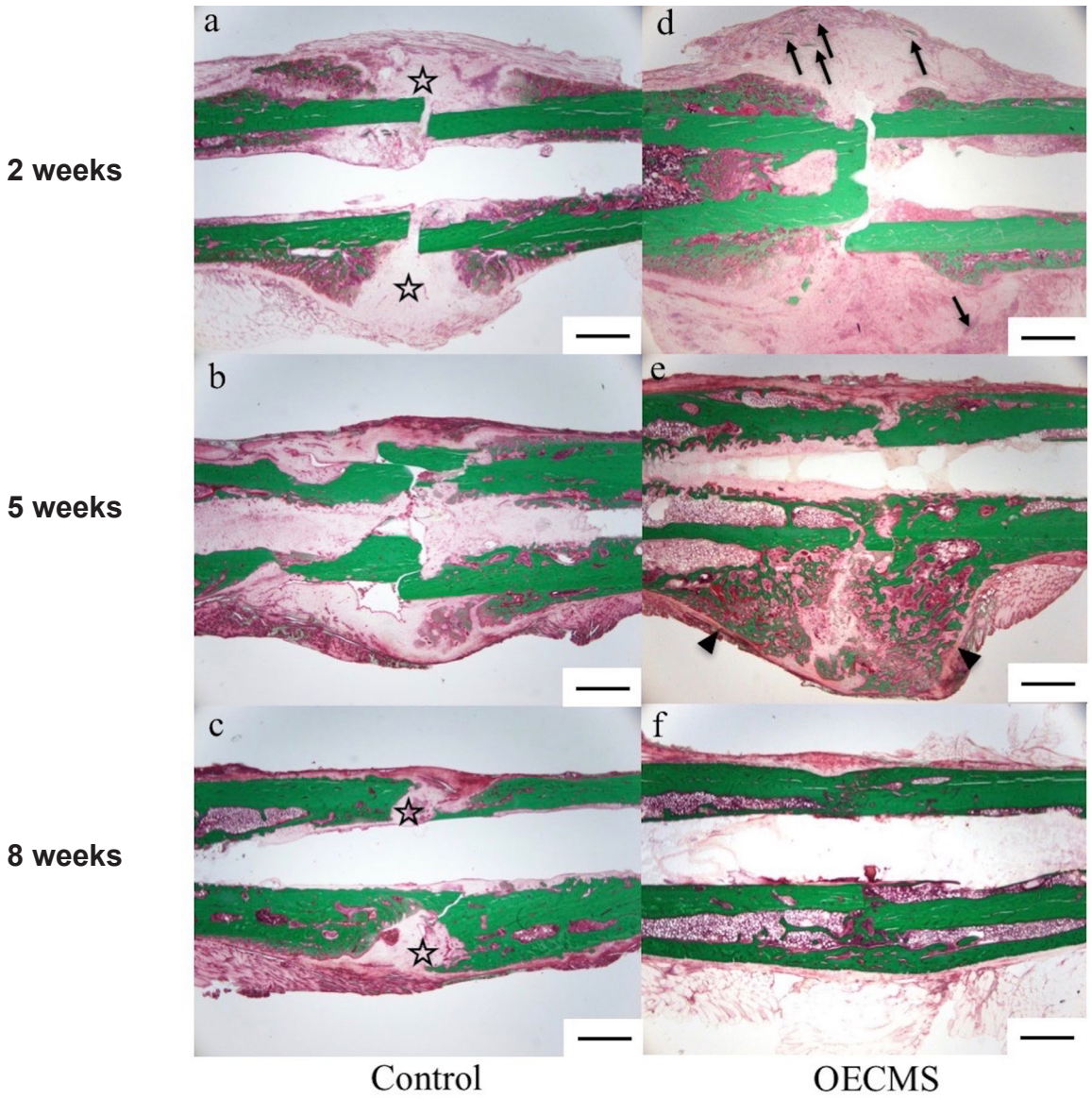

Fig. 6. Histological findings at the fracture sites at 2, 5 and 8 weeks in the OECMS and control groups. (**d**) At 2 weeks, large soft tissue covered the fracture site and the calcification (green staining: black arrow) on its outer layer in the OECMS group; (**a**) however, fibrous tissue (☆) was interposed between the ends of the fractured bone in the control group. (**e**) At 5 weeks, the obvious calcification (green staining: black arrowhead) was expanded onto the periosteum in the OECMS group; (**b**) however, bridging calcification was not confirmed over the fracture site in the control group. (**f**) At 8 weeks, bridging callus over the fracture site was observed in the OECMS group; (**c**) however, fibrous granulation tissue (☆) was interposed at the fracture site and the ends of cortical bone had become rounded in the control group. Scale bars = 500 μm.

inside the HA were induced by the OECMS, which contained various osteogenic growth factors, such as BMP-2, VEGF-A, bFGF and TGF-β1. These results indicated that the OECMS had osteoinductive capacity. The combination of VEGF-A and BMP-2 enhances BMP-2-induced bone formation in a rat model of a critical size bone defect (Patel *et al.*, 2008). Moreover, VEGF-A could also act additively or synergistically with several other growth factors, including TGF-β1 and bFGF. Therefore, the delivery of VEGF-A with osteoinductive factors is an attractive approach to promote bone regeneration (Martino *et al.*, 2015). The OECMS had an osteoinductive but not osteogenic capacity as it was acellularised following the freeze-thaw cycling in liquid nitrogen. The lack of osteocalcin and alkaline phosphatase mRNA expression at 4 weeks after implantation suggested that the HA constructs with OECMS did not contain substantial living osteogenic cells, with no osteocyte and bone tissue formation observed early after implantation.

Over recent years, non-union models in mice or rats have been established (Garcia *et al.*, 2013). Because mice are a species on the lower phylogenetic

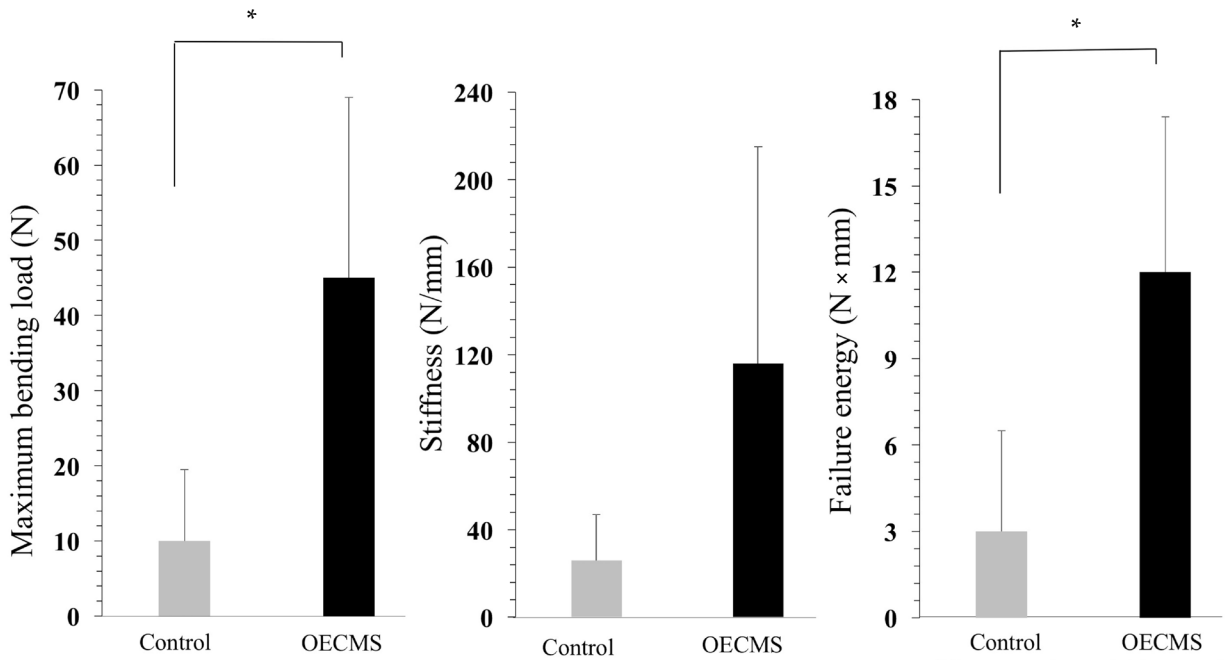

Fig. 7. Biomechanical evaluation using the three-point bending test of rat femoral non-union model at 8 weeks in the OECMS and control groups. Maximum bending load and failure energy in the OECMS group were significantly higher than in the control group (* $p < 0.05$, $n = 6$).

scale, they have a great potential for bone repair and even unstabilised fractures can heal without delay (Colnot *et al.*, 2003). Therefore, rats were used as non-union model in this study. OECMS implantation in the rat non-union model showed enhanced bone regeneration on radiography, histology and biomechanical analysis. On the histological analysis, the amount of the covering tissue on the fracture site of the OECMS group, which included calcification, was much larger than that of the control group 2 weeks after implantation, confirming that the OECMS was still present over the fracture site. The calcification expanded in the OECMS group until the unremoved periosteum 5 weeks after surgery. BMSCs accumulated from the unremoved periosteum, bone marrow and external surrounding soft tissue and migrated into the collagen network of the OECMS, driven by osteogenic growth factors. Thus, the OECMS would be a suitable natural scaffold for bone formation, having demonstrated osteoconductive capacity.

The current study presented some limitations. First, the dead cells included in the OECMS might affect macrophage activation and exacerbate local inflammation during bone regeneration. No allogenic implantation, but preliminary isogenic implantation was analysed to eliminate rejection by the immune system. In future studies, decellularisation will be needed for the clinical application of allogenic implantation. Second, there are several devitalisation methods available to prepare ECM scaffolds (Crapo *et al.*, 2001; Gilbert *et al.*, 2012). The conventional devitalisation methods include the combination of thermal shock, freeze-thaw cycling (Elder *et al.*, 2010; Patel *et al.*, 2008), chemical treatment (Du *et al.*, 2011), osmotic shock and mechanical disruption (Xu *et al.*, 2007). Osmotic shock can readily cause cell lysis with minimal change to the matrix molecules and architecture (Xu *et al.*, 2007). Freeze-thaw cycling does not significantly reduce the ECM proteins nor the mechanical strength of the tissues (Elder *et al.*, 2010; Patel *et al.*, 2008). In the current study, only freeze-thaw cycling was used. For clinical applications, the most suitable method for preparing OECMS will need to be assessed.

Conclusion

The OECMS maintained its sheet structure and contained osteoinductive growth factors, including BMP-2, VEGF-A, bFGF and TGF-β1, after the freeze-thaw cycling in liquid nitrogen. The OECMS resulted to be a sheet-shaped material with rich osteoinductive and osteoconductive capacity and might have a potential as novel scaffold-free material without cell seeding in bone regeneration medicine.

Acknowledgements

The authors thank Fumika Kunda and Miya Matsumura (Nara Medical University Faculty of Medicine, Japan) for their technical assistance. The study was supported by a grant from the Japan Orthopaedics and Traumatology Research

Foundation, Inc. and the Translational Research Network Program from the Japan Agency for Medical Research and Development, AMED.

The authors have no conflicts of interest to disclose.

References

Akahane M, Nakamura A, Ohgushi H (2008) Osteogenic matrix sheet-cell transplantation using osteoblastic cell sheet resulted in bone formation without scaffold at an ectopic site. J Tissue Eng Regen Med **2**: 196-201.

Akahane M, Shigematsu H, Tadokoro M, Ueha T, Matsumoto T, Tohma Y, Kido A, Imamura T, Tanaka Y (2010) Scaffold-free cell sheet injection results in bone formation. J Tissue Eng Regen Med **4**: 404-411.

Antebi B, Zhang Z, Wang Y, Lu Z, Chen XD, Ling J (2015) Stromal-cell-derived extracellular matrix promotes the proliferation and retains the osteogenic differentiation capacity of mesenchymal stem cells on three-dimensional scaffolds. Tissue Eng Part C Methods **21**: 171-181.

Axelrad TW, Einhorn TA (2009) Bone morphogenetic proteins in orthopaedic surgery. Cytokine Growth Factor Rev **20**: 481-488.

Colnot C, Thompson Z, Miclau T, Werb Z, Helms JA (2003) Altered fracture repair in the absence of MMP9. Development **130**: 4123-4133.

Crapo PM, Gilbert TW, Badylak SF (2001) An overview of tissue and whole organ decellularization processes. Biomaterials **32**: 3233-3243.

Discher DE, Mooney DJ, Zandstra PW (2009) Growth factors, matrices, and forces combine and control stem cells. Science **324**: 1673-1677.

Du L, Wu X, Pang K, Yang Y (2011) Histological evaluation and biomechanical characterisation of an acellular porcine cornea scaffold. Br J Ophthalmol **95**: 410-414.

Elder BD, Kim DH, Athanasiou KA (2010) Developing an articular cartilage decellularization process toward facet joint cartilage replacement. Neurosurgery **66**: 722-727.

Even J, Eskander M, Kang J (2012) Bonemorphogenetic protein in spine surgery: current and future uses. J Am Acad Orthop Surg **20**: 547-552.

Farag A, Vaquette C, Theodoropoulos C, Hamlet SM, Hutmacher DW, Ivanovski S (2014) Decellularized periodontal ligament cell sheets with recellularization potential. J Dent Res **93**: 1313-1319.

Fei Y, Gronowicz G, Hurley MM (2013) Fibroblast growth factor-2, bone homeostasis and fracture repair. Curr Pharm Des **19**: 3354-3363.

Giannoudis PV, Einhorn TA, Marsh D (2007) Fracture healing: the diamond concept. Injury **38**: S3-S6.

Gilbert TW (2012) Strategies for tissue and organ decellularization. J Cell Biochem **113**: 2217-2222.

Garcia P, Histing T, Holstein JH, Klein M, Laschke MW, Matthys R, Ignatius A, Wildemann B, Lienau J, Peters A, Willie B, Duda G, Claes L, Pohlemann T, Menger MD (2013) Rodent animal models of delayed bone healing and non-union formation: a comprehensive review. Eur Cell Mater **26**: 1-12.

Hankenson KD, Dishowitz M, Gray C, Schenker M (2011) Angiogenesis in bone regeneration. Injury **42**: 556-561.

Junka R, Yu X (2015) Novel acellular scaffold made from decellularized Schwann cell sheets for peripheral nerve regeneration. Regen Eng Transl Med **1**: 22-31.

Kim BS, Choi JS, Kim JD, Choi YC, Cho YW (2012) Recellularization of decellularized human adipose-tissue-derived extracellular matrix sheets with other human cell types. Cell Tissue Res **348**: 559-567.

Kim IG, Hwang MP, Du P, Ko J, Ha CW, Do SH, Park K (2015) Bioactive cell-derived matrices combined with polymer mesh scaffold for osteogenesis and bone healing. Biomaterials **50**: 75-86.

Kittaka M, Kajiya M, Shiba H, Takewaki M, Takeshita K, Khung R, Fujita T, Iwata T, Nguyen TQ, Ouhara K, Takeda K, Fujita T, Kurihara H (2015) Clumps of a mesenchymal stromal cell/extracellular matrix complex can be a novel tissue engineering therapy for bone regeneration. Cytotherapy **17**: 860-873.

Kito K, Kagami H, Kobayashi C, Ueda M, Terasaki H (2005) Effects of cryopreservation on histology and viability of cultured corneal epithelial cell sheets in rabbit. Cornea **24**: 735-741.

Kokubu T, Hak DJ, Hazelwood SJ, Reddi AH (2003) Development of an atrophic non-union model and comparison to a closed healing fracture in rat femur. J Orthop Res **21**: 503-510.

Komatsu DE, Warden SJ (2010) The control of fracture healing and its therapeutic targeting: improving upon nature. J Cell Biochem **109**: 302-311.

Lau TT, Lee LQ, Vo BN, Su K, Wang DA (2012) Inducing ossification in an engineered 3D scaffold-free living cartilage template. Biomaterials **33**: 8406-8417.

Macri L, Silverstein D, Clark RA (2007) Growth factor binding to the pericellular matrix and its importance in tissue engineering. Adv Drug Deliv Rev **59**: 1366-1381.

Martino MM, Briquez PS, Maruyama K, Hubbell JA. (2015) Extracellular matrix-inspired growth factor delivery systems for bone regeneration. Adv Drug Deliv Rev **94**: 41-52.

Nakamura A, Akahane M, Shigematsu H, Tadokoro M, Morita Y, Ohgushi H, Dohi Y, Imamura T, Tanaka Y (2010) Cell sheet transplantation of cultured mesenchymal stem cells enhances bone formation in a rat non-union model. Bone **46**: 418-424.

Okuda A, Horii N, Sasagawa T, Shimizu T, Shigematsu H, Iwata E, Morimoto Y, Masuda K, Koizumi M, Akahane M, Nishi M, Tanaka Y (2017) Bone marrow stromal cell sheets may promote

axonal regeneration and functional recovery with suppression of glial scar formation after spinal cord transection injury in rats. J Neurosurg Spine **26**: 388-395.

Patel N, Solanki E, Picciani R, Cavett V, Caldwell-Busby JA, Bhattacharya SK (2008) Strategies to recover proteins from ocular tissues for proteomics. Proteomics **8**: 1055-1070.

Pham QP, Kasper FK, Scott-Baggett L, Raphael RM, Jansen JA, Mikos AG (2008) The influence of an *in vitro* generated bone-like extracellular matrix on osteoblastic gene expression of marrow stromal cells. Biomaterials **29**: 2729-2739.

Schindeler A, McDonald M.M, Bokko P. Little DG (2008) Bone remodeling during fracture repair: the cellular picture. Semin Cell Dev Biol **19**: 459-466.

Schultz GS, Wysocki A (2009) Interactions between extracellular matrix and growth factors in wound healing. Wound Repair Regen **17**: 153-162.

Shimizu T, Akahane M, Morita Y, Omokawa S, Nakano K, Kira T, Onishi T, Inagaki Y, Okuda A, Kawate K, Tanaka Y (2010) The regeneration and augmentation of bone with injectable osteogenic cell sheet in a rat critical fracture healing model. Injury **46**: 1457-1464.

Sun Y, Li W, Lu Z, Chen R, Ling J, Ran Q, Jilka RL, Chen XD (2011) Rescuing replication and osteogenesis of aged mesenchymal stem cells by exposure to a young extracellular matrix. FASEB J **25**: 1474-1485.

Takata M, Sugimoto N, Yamamoto N, Shirai T, Hayashi K, Nishida H, Tanzawa Y, Kimura H, Miwa S, Takeuchi A, Tsuchiya H (2011) Activity of bone morphogenetic protein-7 after treatment at various temperatures: freezing *vs.* pasteurization *vs.* allograft. Cryobiology **63**: 235-239.

Tsuchiya H, Wan SL, Sakayama K (2005) Reconstruction using an autograft containing tumour treated by liquid nitrogen. J Bone Joint Surg Br **87**: 218-225.

Xing Q, Yates K, Tahtinen M, Shearier E, Qian Z, Zhao F (2015) Decellularization of fibroblast cell sheets for natural extracellular matrix scaffold preparation. Tissue Eng Part C Methods **21**: 77-87.

Xu CC, Chan RW, Tirunagari N (2007) A biodegradable, acellular xenogeneic scaffold for regeneration of the vocal fold lamina propria. Tissue Eng **13**: 551-566.

Zhang W, Zhu Y, Li J, Guo Q, Peng J, Liu S, Yang J, Wang Y (2016) Cell-derived extracellular matrix: basic characteristics and current applications in orthopedic tissue engineering. Tissue Eng Part B Rev **22**: 193-207.

Discussion with Reviewers

Ana Ferreira: The authors proposed the OECMS as a potential new scaffold-free material for bone tissue engineering. Please explain the motivation of implanting HA constructs (a synthetic bone-mineral-like material) combined with the OECMS?
Authors: In a clinical scenario, it is difficult to obtain complete bone regeneration using a large artificial bone. The OECMS could contribute with its osteoinductive capacity to the artificial bone regeneration, making it possible to treat large bone defects. Therefore, the aim of the current study was to test the bone regeneration capacity of the HA constructs combined with OECMS in a rat model.

Sven Otto: What about the transmission of viral, prionic or other diseases? And the human leukocyte antigen (HLA) sensibilisation potential?
Authors: The freeze-thaw cycling method in liquid nitrogen cannot deactivate the proteins completely. Therefore, viral, prionic or other diseases will still be partially present in the sample. HLA will not be deactivated after freeze-thaw cycling. However, remaining HLA of dead cells will not negatively affect the bone healing in the isogenic implantation.

Editor's note: The Scientific Editor responsible for this paper was Chris Evans.